Geophys. J. Int. (2004) **157,** 1130–1145 doi: 10.1111/j.1365-246X.2004.02264.x

The sensitivity of seafloor compliance measurements to sub-basalt sediments

Wayne C. Crawford

Laboratoire de Géosciences Marines, IPG Paris Case 89, *Tour* 24-25*1ere étage,* 4 *Place Jussieu, Paris* 75252, *France. E-mail: crawford@ipgp.jussieu.fr*

Accepted 2004 January 27. Received 2004 January 27; in original form 2003 March 31

SUMMARY

We investigate the sensitivity of seafloor compliance – the transfer function between the seafloor stress and displacement under ocean waves – to sub-basalt sediments. Seafloor compliance is sensitive to the subsurface shear modulus as a function of depth and is particularly sensitive to low shear modulus regions such as fluid-saturated sediments. We generate synthetic seafloor compliance data for different models of sediments beneath basalts, run geophysical inversions on the data and compare the inversion results with the input models. Our input models are variations on a reference model in which sub-basalt sediments start 3.5 km beneath the seafloor and have an average shear modulus of 6.8×10^9Pa (shear wave velocity *ca* 1.7 km s^{-1}). The sensitivity of seafloor compliance to sub-basalt sediments depends mostly on the water depth and the sub-basalt sediment layer depth, thickness and shear modulus. If the water depth is 1 km or more, seafloor compliance measurements will detect a sub-basalt sediment layer 0.6 km or more thick and will constrain the depth to the top and bottom of a 2-km thick sub-basalt sediment layer to within 0.2 km. If the water depth is 0.25 km, the thinnest detectable layer will be 1.2 km and the depth uncertainty for a 2-km thick sub-basalt sediment layer will be 0.5–0.8 km. Neither interlayered sediments within the basalts nor sediments above the basalt layer have a strong effect on the measurement sensitivity.

Key words: seafloor compliance, sediments, seismic, shear modulus, sub-basalt.

1 INTRODUCTION

Eruptive basalt flows over sedimentary basins may trap rich hydrocarbon reservoirs at several volcanic margins, including sites in the North Atlantic ocean, off the coast of West Africa and offshore India. These sites are often in deep water and the sub-basalt sediments often sit several km beneath the seafloor. Despite the difficult access to these sites and the potentially high cost of drilling through the overlying basalt cap, the potential of these reservoirs has stimulated significant research using a variety of geophysical methods. Ocean Bottom Seismometer (OBS) tomography and large-offset streamer experiments have had the most success, revealing sub-basalt sediments and constraining their large-scale compressional velocity (Hughes *et al.* 1997, 1998; Fruehn *et al.* 1999; White *et al.* 1999; Fliedner & White 2001). Small-offset seismic reflection methods are hindered by the high impedance contrast and scattering at the basalt layer surface, as well as scattering within the basalt layer as a result of sediment interfingering (Gatliff *et al.* 1984; Mack 1997; Ogilvie *et al.* 2001). Lower frequency seismic sources may provide better small-offset penetration at the cost of decreased resolution (Hobbs 2002; Ziolokowski *et al.* 2002). Magnetotellurics (Jegen *et al.* 2002), controlled source electromagnetics (MacGregor & Sinha 2002) and gravity gradients (Murphy 2002) have also been proposed to image sub-basalt sediments.

In this paper, we investigate the sensitivity of seafloor compliance measurements to sub-basalt sediments. Seafloor compliance is a relatively new geophysical prospecting technique that uses the seafloor deformation under ocean waves to determine the subsurface shear modulus (Yamamoto & Torii 1986, 1989; Crawford *et al.* 1991, 1998; Latychev & Edwards 2003). Seafloor compliance is the transfer function between the seafloor pressure and displacement fields as a function of frequency. It is measured by deploying a broad-band seismometer and differential pressure gauge to the seafloor for two or more days. Multiple seafloor compliance measurements can be used to create 2-D or 3-D subsurface shear modulus models. Seafloor compliance measurements are most sensitive to low shear modulus regions and are insensitive to impedance contrasts such as reflectors in the basalt layer. The sensitivity of seafloor compliance measurements to the subsurface shear modulus complements the sensitivity of active seismic experiments to compressional wave velocities and acoustic impedance contrasts.

We calculate the sensitivity of seafloor compliance measurements to sub-basalt sediments by running geophysical inversions on synthetic seafloor compliance data calculated for a range of subsurface models and environmental and experimental conditions. The subsurface models are variations on a reference model compiled from seismic data in the central and northwestern Faeroes basin, where Palaeocene–Eocene

basalt flows from the Faeroe Islands overly thick Mesozoic and Tertiary sedimentary sequences (Ridd 1981; Mudge & Rashid 1987; Hughes *et al.* 1997, 1998; Fruehn *et al.* 1999; White *et al.* 1999; Fliedner & White 2001). For each model and set of conditions, we compare the inversion results to the starting models to constrain the seafloor compliance sensitivity to sub-basalt sediments and to identify the factors controlling this sensitivity.

2 SEAFLOOR COMPLIANCE

2.1 Seafloor compliance equations and behaviour

We define seafloor compliance as the seafloor displacement, $\mathbf{u}(\omega, 0)$, divided by the vertical seafloor stress, $\tau_{zz}(\omega, 0)$, multiplied by the wavenumber, $k_w\,(\omega)$, of the stress field, all as a function of frequency:

$$\eta(\omega) \equiv k_w(\omega)\frac{\mathbf{u}(\omega, 0)}{\tau_{zz}(\omega, 0)}. \tag{1}$$

To calculate the seafloor compliance of a given seafloor model, we solve the seismic equation of motion:

$$\rho\ddot{u}_i = \tau_{ij,j}, \tag{2}$$

where ρ is the material density, u_i is the motion in the i direction and τ_{ij} is the stress acting in the j direction across the plane normal to the i-axis.

For a 1-D, isotropic, stratified model under plane wave forcing, eq. (2) leads to upgoing and downgoing P and SV waves whose amplitude varies with depth in each layer as

$$\begin{aligned} &\exp(\pm r_i z), \quad r_i = k_w\sqrt{1 - c_w^2/\alpha_i^2}, \quad \alpha_i = \sqrt{\frac{\lambda_i + 2\mu_i}{\rho_i}}, \\ &\exp(\pm s_i z), \quad s_i = k_w\sqrt{1 - c_w^2/\beta_i^2}, \quad \beta_i = \sqrt{\frac{\mu_i}{\rho_i}}, \end{aligned} \tag{3}$$

where α_i is the compressional wave velocity in layer i, β_i is the shear wave velocity, μ_i is the shear modulus, λ_i is the dilatation modulus, ρ_i is the density and we set $z = 0$ at the seafloor (Aki & Richards 1980). If the forcing waves are slower than the subsurface shear wave velocity, r_i and s_i are real positive and the P-SV waves are evanescent. If c_w is much less than β_i, then r_i and s_i are approximately equal to k_w.
The seafloor stress field used for seafloor compliance measurements is the pressure from linear ocean surface gravity waves (Fig. 1), whose wavenumber is related to the frequency, f, and the water depth, H, by the dispersion equation

$$\omega^2 = gk\tanh(k_w H), \tag{4}$$

where $\omega = 2\pi f$ is the angular frequency and g is the gravitational acceleration (Apel 1987). These waves travel much slower than typical subsurface seismic wave velocities: less than 0.03 km s^{-1}at 0.1 km water depth and less than 0.2 km s^{-1}at 4 km water depth. For a 2-km water depth and assuming $\beta_i > 0.5$ km s^{-1}, $0.96\,k < s_i < k$ and $0.996k_w < r_i < k_w$.

We calculate seafloor compliance from eqs (1–3) by imposing zero motion at infinite depth, free slip at the seafloor and matching stresses and motions across layer boundaries. For an isotropic uniform half-space under quasi-static plane wave forcing, the seafloor compliance is

$$\eta(\omega) = \frac{-i}{2(\lambda + \mu)}\hat{x} + \frac{(\lambda + 2\mu)}{2\mu(\lambda + \mu)}\hat{z}, \tag{5}$$

where the pressure field is assumed to propagate in the x-direction (see the Appendix). The vertical motion is at least five times more sensitive to μ than to λ (Crawford *et al.* 1991) and this sensitivity increases as μ/λ decreases (Fig. 2). If $\mu \ll \lambda$, then the vertical motion is inversely proportional to μ. This result is confirmed by computer modelling that includes the elastodynamic terms (Crawford *et al.* 1998). Although both horizontal and vertical motions are excited by the source waves, only the vertical motions have been successfully measured at the seafloor because the horizontal noise levels are much higher as a result of current-induced instrument tilting (Crawford & Webb 2000). For the rest of this paper, seafloor compliance refers only to the vertical term.

We calculate seafloor compliance for 1-D models using a minor vector implementation of the propagator method developed for P-SV waves (Gomberg & Masters 1988; Crawford *et al.* 1991). The inertial terms (the left side of eq. 2) may have some effect on seafloor compliance, especially if there are low shear modulus regions in the subsurface, so we always solve the full equations of motion. For most realistic subsurface models, the result is indistinguishable from that obtained using only the static terms. For 2-D and 3-D models, seafloor compliance has been calculated using finite difference approximations (Crawford *et al.* 1998; Latychev & Edwards 2003).

Whether the model is 1-D, 2-D or 3-D, seafloor compliance is most sensitive to $1/\mu$ (Crawford *et al.* 1991; Crawford *et al.* 1998; Latychev & Edwards 2003). Seafloor compliance at a given frequency is most sensitive to the elastic parameters at a depth between $1/2\pi$ and $1/4$ the water wavelength (Crawford *et al.* 1998). Because the wavelength of the source infragravity waves increases with decreasing frequency, seafloor compliance is sensitive to deeper depths at lower frequencies. Therefore, if the subsurface shear modulus increases with depth, seafloor compliance will increase with frequency (Fig. 3). A low shear modulus region such as a melt body, a fluid pocket, or sediments beneath a basalt flow will generate a seafloor compliance peak centred at the frequency corresponding to the region's depth.

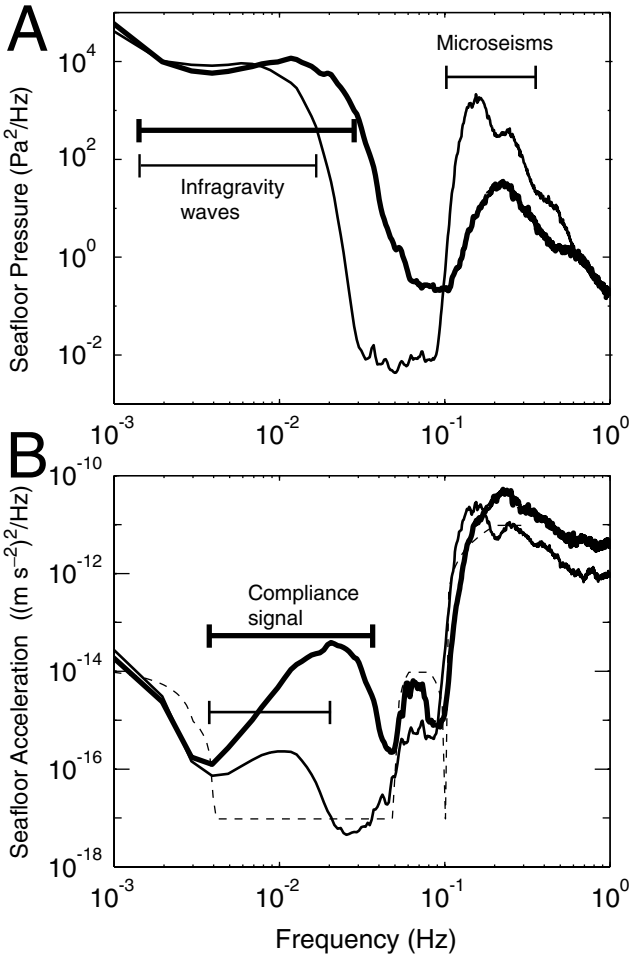

Figure 1. Seafloor pressure and acceleration power spectral densities (PSDs) measured at two Pacific ocean sites. A sedimented seafloor site at 0.9-km water depth (thick line). A rocky seafloor site at 2.6-km water depth (thin line). The infragravity wave and microseism frequency bands are labelled. (a) Pressure PSDs. (b) Acceleration PSDs. Seafloor compliance creates the acceleration peaks between 0.003 and 0.03 Hz. The background noise level we use to calculate synthetic seafloor compliances (dashed line).

2.2 The seafloor compliance frequency band

Seafloor compliance is measured in the frequency band from 0.003 to approximately 0.03 Hz. The low frequency limit is imposed by a rapid increase in seismic noise below 0.004 Hz (Fig. 1b), while the water depth controls the high frequency limit, which corresponds empirically to the frequency at which $\lambda_w \equiv 2\pi/k_w = 1.1H$. The seafloor pressure signal, $P(H)$, under linear ocean surface gravity waves is related to the near-surface pressure, $P(0)$, by the equation:

$$\frac{P(H)}{P(0)} = \frac{1}{\cosh(k_w H)}, \tag{6}$$

corresponding to an exponential decay in pressure with depth (Apel 1987). For $\lambda_w > 2\pi H$, $P(H)$ is at least 2/3 of $P(0)$, but for $\lambda_w = H$ it is 267 times smaller and for $\lambda_w = H/2$ it is 143 000 times smaller.

At water depths greater than 0.2 km, most of the seafloor linear wave energy comes from infragravity waves, which are generated by wind waves through non-linear wave–wave interactions (Longuet-Higgins 1950). Infragravity waves start out as non-linear forced waves, which form the envelope of wind wave groups, and are converted to linear free waves through shoaling processes at coastlines (Webb *et al.* 1991). Most of this energy is refractively trapped at the coastlines, but some of it leaks into the deep ocean, where it can traverse ocean basins with little attenuation. At water depths greater than 0.1 km, more than 99 per cent of the seafloor infragravity wave pressure field comes from linear waves (Webb *et al.* 1991; Okihiro *et al.* 1992; Crawford 1994). Open ocean infragravity waves are 0.3 to 10 mm tall and up to several tens of km in wavelength. While ocean surface wind waves are usually much taller than infragravity waves, almost all of their energy is at wavelengths shorter than 0.2 km and so they generate little or no deep ocean pressure signal. Deep ocean infragravity wave power spectral densities range from $10^{2.5}$ to $10^{5.2}$ Pa^2 Hz. Infragravity waves are relatively strong (10^4–$10^{5.2}$ Pa^{2}Hz) and steady in the Pacific ocean, and weaker and more variable in the Atlantic ocean. This may be because sites in the Atlantic ocean are not within a direct wave propagation path from as much high-latitude shoreline as Pacific sites. The principal Atlantic ocean infragravity wave measurements come from a site that is

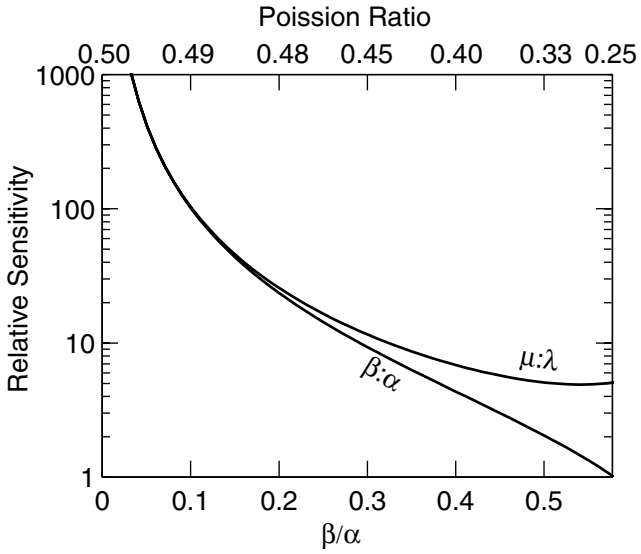

Figure 2. The relative sensitivity of seafloor compliance measurements to elastic parameters. The curves indicate how many times more sensitive seafloor compliance is to the first parameter than to the second (Crawford *et al.* 1998). β is the shear wave velocity, α is the compressional wave velocity.

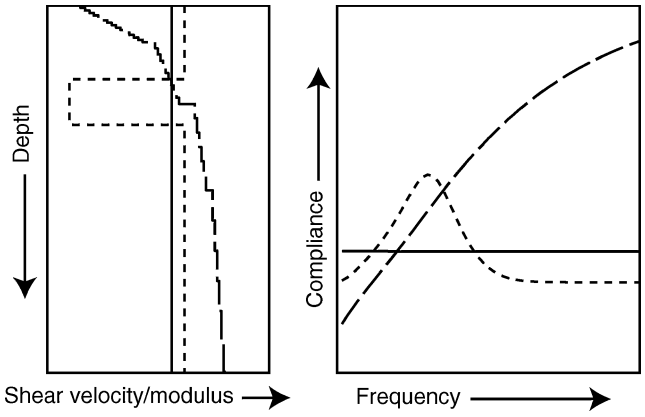

Figure 3. Seafloor compliance of some simple 1-D models: uniform half-space (solid line), normal oceanic crust (long dashes), buried low velocity zone (short dashes).

shielded from waves originating at latitudes above 42°N, and therefore may not be representative of the wave energies at sites that are open to ocean surface waves originating at higher latitudes (Webb *et al.* 1991).

We do not use the microseism band from approximately 0.1–2 Hz for compliance measurements. The energy in this band is divided between local non-linear wave–wave interactions (Longuet-Higgins 1950), local wave–slope interactions (Hasselmann 1963) and seismic interface waves that propagate from stormy regions that have high local microseisms (Webb 1992). The pressure–acceleration transfer function for the seismic waves is not the seafloor compliance but rather the acoustic wave relation: pressure–acceleration $= -k\ /(\omega^2 \rho_w \tanh(kH))$ (where ρ_w is the water density and k is the wavenumber Webb 1998). One might be able to calculate seafloor compliance if the local component could be separated from the seismic waves and the local wavenumbers calculated, but these wavenumbers depend on the direction and amplitude of interfering surface wind waves and probably vary too rapidly to be accurately estimated.

We can calculate the depths to which seafloor compliance is sensitive from the water depth and the data frequency band. For a 0.25-km water depth, the water wavelength is 12 km at 0.004 Hz and 0.3 km at 0.075 Hz, so seafloor compliance is most sensitive to structure between 0.1 and 2 km beneath the seafloor (kmbsf). For a 1-km water depth, seafloor compliance is sensitive to structure between 0.2 and 4 kmbsf and, for a 2-km water depth, seafloor compliance is sensitive to structure between 0.5 and 6 kmbsf.

2.3 Measuring seafloor compliance

We measure seafloor compliance by deploying a four-component broad-band seismometer to the seafloor. The pressure component is measured using a differential pressure gauge (Cox *et al.* 1984). We leave the instrument at the seafloor long enough to collect at least 100 1024-s time-series windows (approximately 29 hr) without earthquake signals after the instrument has levelled and equilibrated to seafloor temperatures. We find that a 42-hr bottom time, corresponding to one measurement every two days, is almost always sufficient. Once the data are recovered,

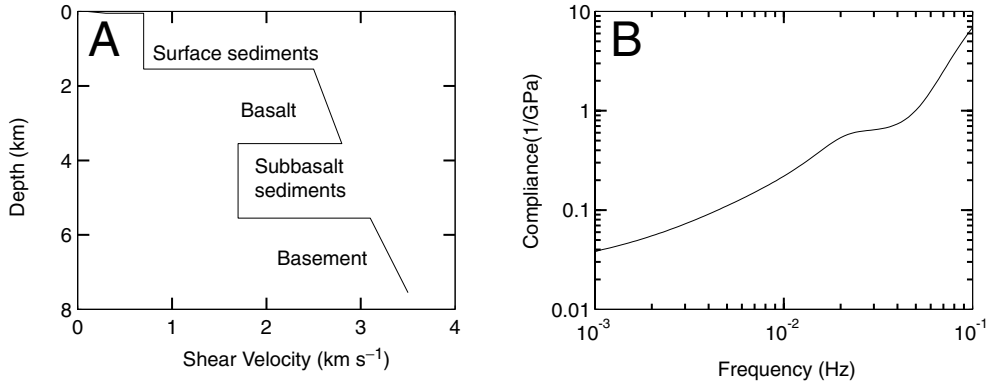

Figure 4. The reference sub-basalt sediment model: (a) shear velocity as a function of depth, (b) seafloor compliance as a function of frequency for a water depth of 1.3 km.

we first remove the effect of the gravitational attraction of the infragravity waves (Crawford *et al.* 1998) and any tilting effects (Crawford & Webb 2000) from the vertical displacement channel. The measured seafloor compliance is

$$\hat{\eta}(\omega) = \frac{k_w(\omega)\gamma(\omega)}{\omega^2}\sqrt{\frac{|S_a(\omega)|}{|S_p(\omega)|}}, \tag{7}$$

where S_a (ω) is the acceleration spectrum and S_p (ω) is the pressure spectrum. We estimate the uncertainty as

$$\varepsilon[|\hat{\eta}(\omega)|] = \frac{[1-\gamma^2(\omega)]^{1/2}}{|\gamma(\omega)|\sqrt{2n_d}}|\hat{\eta}(\omega)|, \tag{8}$$

where γ (ω) is the pressure–acceleration coherence and n_d is the number of data windows (Bendat & Piersol 1986; Crawford *et al.* 1991).

3 METHODS

To determine the seafloor compliance sensitivity to sub-basalt sediments, we simulate seafloor compliance measurements over models containing a sub-basalt sediment layer. We then run geophysical inversions on the simulated data and compare the initial models to the inversion results. All of our test models are derived from the reference model described below.

3.1 The reference sub-basalt sediment model

The reference model consists of 1.5 km of surface sediments, a 2.0-km thick basalt section and 2.0 km of sub-basalt sediments (Fig. 4 and Table 1), which is a simplified version of the depth structure inferred within Faeroes basin from wide-angle seismic experiments (White *et al.* 1999). Because subsurface shear wave velocities are not well constrained by the seismic data, we use shear wave velocities consistent with empirical and theoretical models and with shear velocities measured at other seafloor sites. Where there is a range of possible shear wave velocity values, we chose the values that should best hide sub-basalt sediments from seafloor compliance measurements: that is, the slowest probable shear velocities outside of the sub-basalt sediments and the fastest probable shear velocities within these sediments. In the upper sediments, shear wave velocities increase from 0.1 km s^{-1} at the seafloor to 0.3 km s^{-1} at 0.05 km depth and are constant at 0.7 km s^{-1} from 0.05 to 1.5 km depth. These values are at the low end of sediment shear velocities measured at seafloor sites (Hamilton 1976; Collins *et al.* 1996; Dorman 1997; Tinivella & Accaino 2000). The basalt layer shear velocity corresponds to a Poisson ratio of 0.28, which is a common value for altered basalts. Within the sub-basalt sediments, we assume a Poisson ratio of 0.35, which is at the low end of estimates for non-dry sediments at high pressures (Stoll 1977; Tinivella & Accaino 2000).

Table 1. The reference sub-basalt sediment model. Unless otherwise stated, we calculate seafloor compliance assuming a 1.3-km water depth, 10^4 Pa^2 Hz infragravity wave energy and 100 1024-s.

Level	Thickness (km)	Density (kg m^{-3})	V_P (km s^{-1})	V_S (km s^{-1})	μ (GPa)
First sediment layer	0.05	1.2–1.8	1.7	0.1–0.3	0.01–0.16
Second sediment layer	1.45	2	1.7	0.7	1.0
Basalts	2	2.45	4.5–5.0	2.5–2.8	15–19
Sub-basalt sediments	2	2.35	3.6	1.7	6.8
Basement gradient	2	2.65	5.2–6.2	3.1–3.5	25–32
Basement half-space	Infinite	2.65	6.2	3.5	32

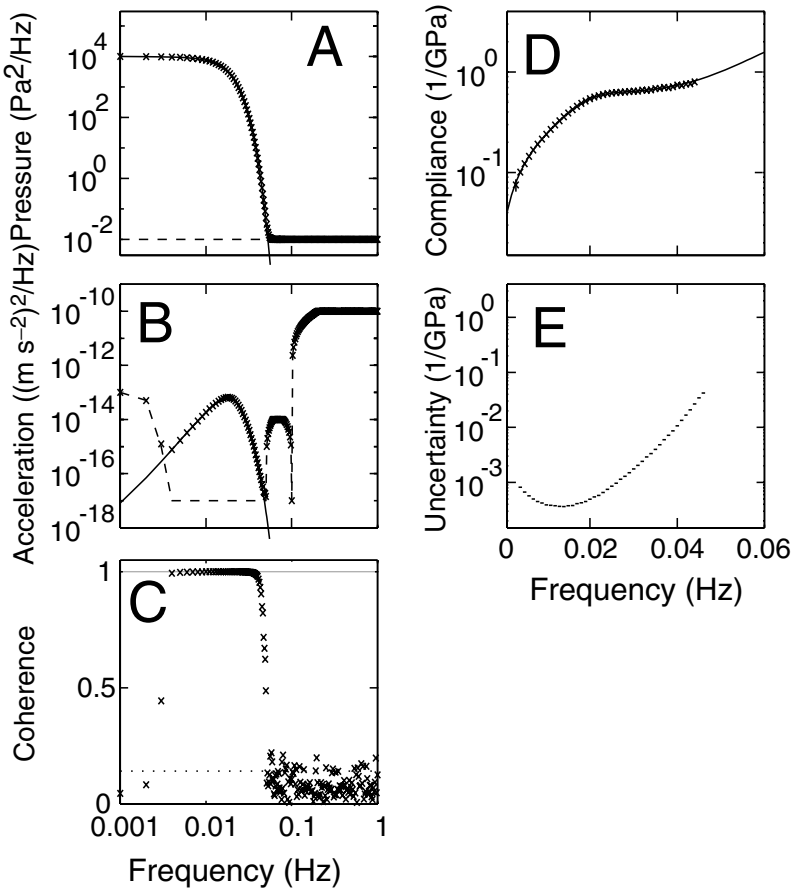

Figure 5. Synthetic pressure and acceleration spectra, coherences and seafloor compliance measurements, calculated using the reference model (Fig. 4 and Table 1). (a) Seafloor pressure spectrum: solid line shows the signal from the source waves, dashed line shows instrument noise, symbols show measured pressure (pressure plus noise). (b) Seafloor acceleration spectrum: solid line shows the signal created by seafloor compliance, dashed line shows environmental noise, symbols show measured acceleration. (c) Coherence between the measured pressure and acceleration. Dotted line shows the 95 per cent significance level. (d) Seafloor compliance: solid line shows theoretical values, symbols show measured values. (e) Seafloor compliance uncertainties calculated from the coherence and number of data windows (eq. 8).

We made the reference model as simple as possible, so that we could isolate the effect of each model parameter. In general, seafloor compliance is not sensitive to small-scale, small-amplitude variations in sub-surface structure, so our results should be valid for more complicated subsurface structures. For example, seismic data and drilling indicate that numerous basalt flows are interbedded with sediments within the basalt layer, but repeated experimentation shows that their seafloor compliance can always be fit with a smooth model such as the one we present.

3.2 Simulating seafloor compliance measurements

We simulate seafloor compliance measurements by calculating the seafloor acceleration under a typical seafloor pressure signal, then adding typical environmental and instrumental noise to the pressure and acceleration signals (Fig. 5). Our seismic noise model (dashed line, Figs 1 and 5b) is based on seafloor acceleration measurements by Beauduin *et al.* (1996), Bradley *et al.* (1997), Collins *et al.* (1998), Crawford *et al.* (1999), Stephen *et al.* (1999) and Webb & Crawford (1999). Other reference values are:

(i) 1.3-km water depth;
(ii) 10^4 Pa^2 Hz sea surface infragravity wave pressure power spectral density;
(iii) 28 hr of good data (100 1024-s data windows).

For each model and set of environmental conditions, we generate pressure and acceleration spectra by adding random (Gaussian) noise equivalent to our noise models to seafloor pressures calculated using a constant P (0) and eq. (6) and to acceleration spectra calculated from the seafloor pressure and the seafloor compliance using eq. (1). We then calculate synthetic seafloor compliance from these spectra using eqs (7) and (8).

3.3 Inversions

We calculate shear modulus/velocity models from the synthetic seafloor compliance data using geophysical inversions based on either minimum structure or *a priori* (Bayesian) constraints. The minimum structure inversions indicate the sensitivity of seafloor compliance to the sub-basalt sediments in the absence of prior constraints, while the Bayesian inversions indicate how seafloor compliance measurements are improved by (and improve) prior data. Typically, these prior data will be layer depths and some velocity information from seismic studies. We use an iterative scheme based on a formal linear inversion, in which we parametrize the subsurface model by an N-dimensional model vector $\mathbf{m}$, and the simulated seafloor compliance data by an M-dimensional data vector $\mathbf{d} = \mathbf{y} + \boldsymbol{\sigma}_D$, where $\mathbf{y}$ is the model response and $\boldsymbol{\sigma}_D$ is the measurement error. We treat the non-linear seafloor compliance forward problem as linear within each iteration:

$$\mathbf{y} = \mathbf{G}\mathbf{m}, \tag{9}$$

where $\mathbf{G}$ is an MxN matrix relating the response to the model. If we wish to invert for a subset of the model parameters $\mathbf{m}'$, we only calculate $\mathbf{G}$ for these parameters. We hold the layer thicknesses, compressional velocities and densities constant and invert for the model shear modulus or velocity. The density has almost no effect on the seafloor compliance (see eq. 5) and the compressional velocity has a smaller effect than the shear velocity, especially if $\beta/\alpha < 0.4$ (Poisson ratio >0.4). The data misfit is

$$\mathbf{X}^2 = \|\mathbf{W}_D\mathbf{d} - \mathbf{W}_D\mathbf{G}\mathbf{m}'\|^2, \quad \mathbf{W}_D = \begin{bmatrix} \frac{1}{\hat{\sigma}_{D1}} & & & 0 \\ & \frac{1}{\hat{\sigma}_{D2}} & & \\ & & \cdots & \\ 0 & & & \frac{1}{\hat{\sigma}_{DM}} \end{bmatrix}, \tag{10}$$

where $\hat{\sigma}_D$is our estimate of $\boldsymbol{\sigma}_D$. Representing the constraint to be minimized by C, we construct a functional:

$$U = C + \mu_L^{-1}\left(X^2 - X_*^2\right), \tag{11}$$

where X_*^2 is the desired misfit and we choose the Lagrange multiplier μ_L^{-1} to satisfy the misfit term while minimizing the constraint. The optimal $\mathbf{m}'$ is that for which

$$\nabla_{m'} U = 0. \tag{12}$$

For the minimum structure inversion, we construct a model consisting of many thin layers. The constraint is the Euclidean norm of the model second differences:

$$C = R_2 = \|\partial^2\mathbf{m}'\|, \quad \partial^2 = \begin{bmatrix} -1 & 2 & -1 & \cdots & & & & 0 \\ & -1 & 2 & -1 & & & & \\ & & & & \cdots & & & \\ & & & & & -1 & 2 & -1 \\ 0 & & & & & & -1 & 2 & -1 \end{bmatrix}. \tag{13}$$

The solution to eq. (12) is then

$$\mathbf{m}' = \left[(\mathbf{W}\mathbf{G})^T\mathbf{W}\mathbf{G} + \mu\partial^{2^T}\partial^2\right]^{-1}(\mathbf{W}\mathbf{G})^T\mathbf{W}\mathbf{d}. \tag{14}$$

We make the layers thinner than the seafloor compliance resolution, so that the inversion can fit any detectable subsurface structure. For this study, we set the top layer thickness to 0.05 km and increased each subsequent layer thickness by a factor of 1.1. We can invert for either the shear velocity or the shear modulus and calculate the other using the density model, but only the parameter inverted for will be smooth if the density model is discontinuous. We invert for the shear velocities because they are easier to compare with compressional velocities from seismic experiments.

For the Bayesian scheme, we divide the model into a few discrete layers and invert for the shear modulus in each layer and the depths of the layer boundaries. We can invert for either shear modulus or shear velocity because converting between the two parameters introduces no extra structure. We invert here for the shear modulus because it is more closely related to the seafloor compliance. We start with an *a priori* model $\mathbf{m}'_{a\ priori}$ containing estimates of the shear modulus in each layer, the depth to each layer boundary and the uncertainties of these values, $\boldsymbol{\sigma}_M$. The inversion constraint is then the deviation from $\mathbf{m}'_{a\ priori}$:

$$C = \|\mathbf{W}_m\mathbf{m}' - \mathbf{W}_m\mathbf{m}'_{a\ priori}\|^2, \quad \mathbf{W}_m = \begin{bmatrix} \frac{1}{\sigma_{m1}} & & & 0 \\ & \frac{1}{\sigma_{m2}} & & \\ & & \cdots & \\ 0 & & & \frac{1}{\sigma_{mN}} \end{bmatrix}, \tag{15}$$

and the solution to eq. (12) is

$$\mathbf{m}' = \mathbf{m}'_{a\ priori} + \left[(\mathbf{WG})^T\mathbf{WG} + \mu\mathbf{W}_m^2\right]^{-1}(\mathbf{WG})^T\mathbf{W}(\mathbf{d} - \mathbf{G}\mathbf{m}'_{a\ priori}). \tag{16}$$

Because the boundary depths are part of the inversion model and there is no smoothing constraint, we divide the model into as few layers as possible.

We iteratively search for the best model by calculating the linear solution around a starting model, $\mathbf{m}'_0$, updating $\mathbf{m}'_0$ and repeating until the solutions converge. In each iteration, we set $\mathbf{G}$ equal to the Jacobian matrix:

$$G_{ij} = J_{ij} \equiv \frac{\partial F_i(\mathbf{m}'_0)}{\partial \mathrm{m}'_{0j}}. \tag{17}$$

There are several ways to improve the iteration convergence and stability, usually by tuning the distance that the inversion steps from the previous model. We use pre-existing stable iteration algorithms for the minimum structure (Constable *et al.* 1987) and Bayesian (Jackson & Matsu'ura 1985) inversions.

The marginal uncertainty of the Bayesian inversion result can be estimated from the diagonals of the posterior covariance matrix

$$\mathbf{C} = \left[(\mathbf{WG})^T\mathbf{WG} + \mu\mathbf{W}_m^2\right]^{-1} \tag{18}$$

(Jackson & Matsu'ura 1985). This estimator accurately represents the model uncertainty if the relationship between the model and the seafloor compliance is approximately linear in the solution region and if the correlation between two parameters does not depend on the other parameters. We cannot use this estimator for the minimum structure inversions because the constraint functional (eq. 13) explicitly correlates the model parameters (Parker 1994).

4 ANALYSIS

We first analyse the seafloor compliance sensitivity by applying minimum structure and Bayesian inversions to synthetic seafloor compliance data calculated for the reference model. We then apply the Bayesian inversion to synthetic data calculated for different water depths, pressure signal strengths and subsurface models to determine the effect of each parameter. For all inversions, we set $X_*^2 = M$ (the number of data points), corresponding to a weighted RMS misfit of 1. We generally set the model compressional velocity and density to their correct values, but we also investigated the effect of using incorrect values.

4.1 Minimum structure inversions of data from the reference model

Minimum structure inversions detect the reference model sub-basalt sediment layer and constrain its depth bounds to within 0.5–1 km (thick solid line, Fig. 6). Because the depth to the top of the basalt layer is often well constrained by seismic data, we ran a second inversion in which

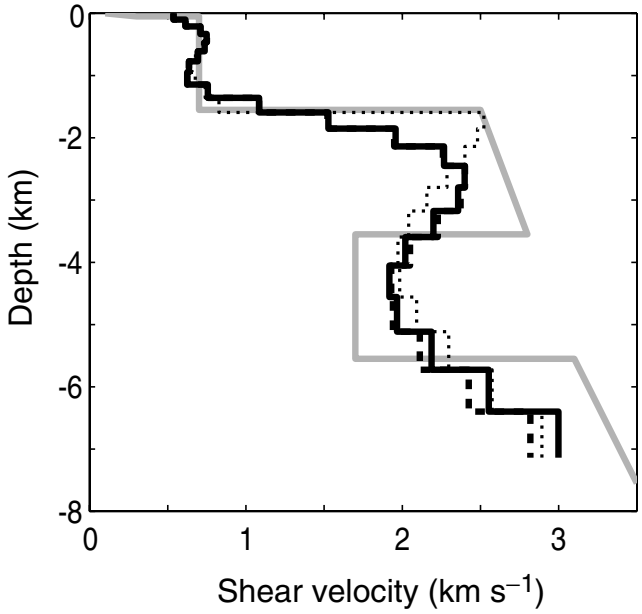

Figure 6. Minimum structure inversion results for simulated seafloor compliance data calculated from the reference model: reference subsurface model (grey line), inversion result for a starting model containing sub-basalt sediments (thick solid line), inversion result for a starting model without sub-basalt sediments (thick dashed line), inversion result when a shear modulus discontinuity is allowed at the interface between the basalts and the overlying sediments (thin dotted line).

Table 2. Variable parameters and *a priori* uncertainties in the Bayesian inversions.

	Parameter	True value	*A priori* uncertainty
Shear modulus in:	First sediment layer	0.06 GPa (0.2 km s^{-1})	0.03 GPa (0.05 km s^{-1})
	Second sediment layer	0.98 GPa (0.7 km s^{-1})	0.28 GPa (0.1 km s^{-1})
	Basalts	17.9 GPa (2.7 km s^{-1})	1.3 GPa (0.1 km s^{-1})
	Sub-basalt sediments	6.8 GPa (1.7 km s^{-1})	1.0 GPa (0.15 km s^{-1})
	Top basement layer	29.7 GPa (3.35 km s^{-1})	1.8 GPa (0.1 km s^{-1})
	Bottom basement layer	32.5 GPa (3.5 km s^{-1})	0.9 GPa (0.05 km s^{-1})
Depth to top of:	Second sediment layer	0.05 km	0.02 km
	Basalts	1.5 km	0.1 km
	Sub-basalt sediments	3.5 km	1.0 km
	Top basement layer	5.5 km	1.0 km

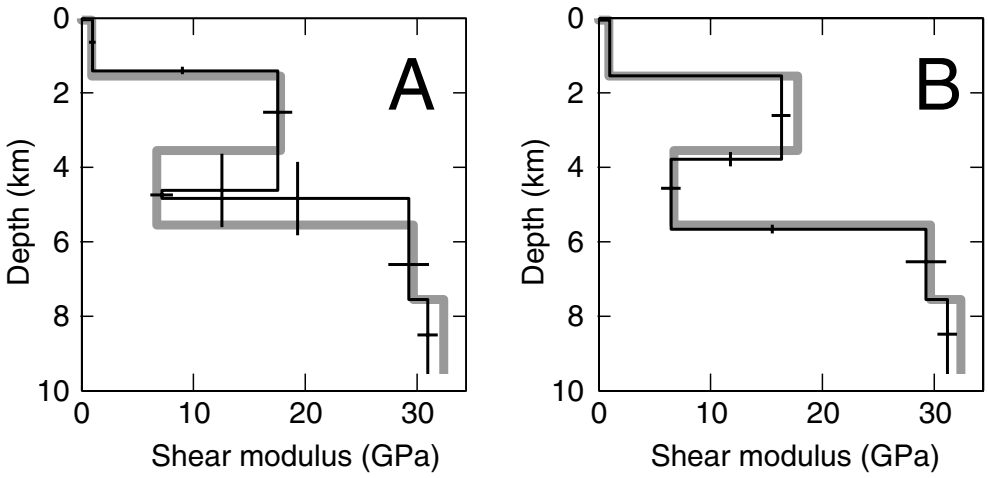

Figure 7. Result of one Bayesian inversion using an *a priori* model in which the sub-basalt sediment layer is much too thin. The thick grey line shows the true model. (a) Starting model and assumed uncertainty. (b) Inversion result and uncertainty.

we allowed the shear velocity to jump at the top of the basalts. The resulting inversion (thin dotted line, Fig. 6) improves the fit to the basalt layer velocities but not to the sub-basalt sediments.

To determine if the assumed compressional velocities and densities affect our results, we ran a third inversion on the same data from which we removed the sub-basalt sediments from the starting model. The result (thick dashed line, Fig. 6) is almost identical to that for the correct starting model, indicating that the choice of compressional velocities and densities has little effect on the inversion results.

4.2 Bayesian data inversions using the reference model

For the Bayesian inversions, we created a six-layer model consisting of a thin surface sediment layer, a thicker near-surface sediment layer, a basalt layer, a sub-basalt sediment layer and two basement layers (Table 2). To minimize the number of variables, we assumed a constant velocity in each layer. We defined 10 variables: the shear modulus in each layer and the depth to the interface between all but the two basement layers. We assigned an *a priori* uncertainty to each variable and built starting models by adding Gaussian noise with standard deviation equal to the *a priori* uncertainty to the true models. Fig. 7 shows an inversion result for a starting model whose sub-basalt sediment layer is too thin. The inversion recovers the layer thickness and boundary depths to within 0.2 km, in agreement with the marginal model uncertainty estimate (eq. 18).

To determine the sensitivity of seafloor compliance to the sub-basalt sediments, we ran one hundred or more inversions per input model, each time regenerating the random (Gaussian) noise in the starting model and seafloor compliance data. We then calculated the mean and variance of the models obtained by the inversions (Fig. 8). The inversions improve the depth constraints in all layers as well as the shear modulus constraint in the second sediment layer. The depth uncertainty to the top and bottom of the sub-basalt sediments decreases from 1.0

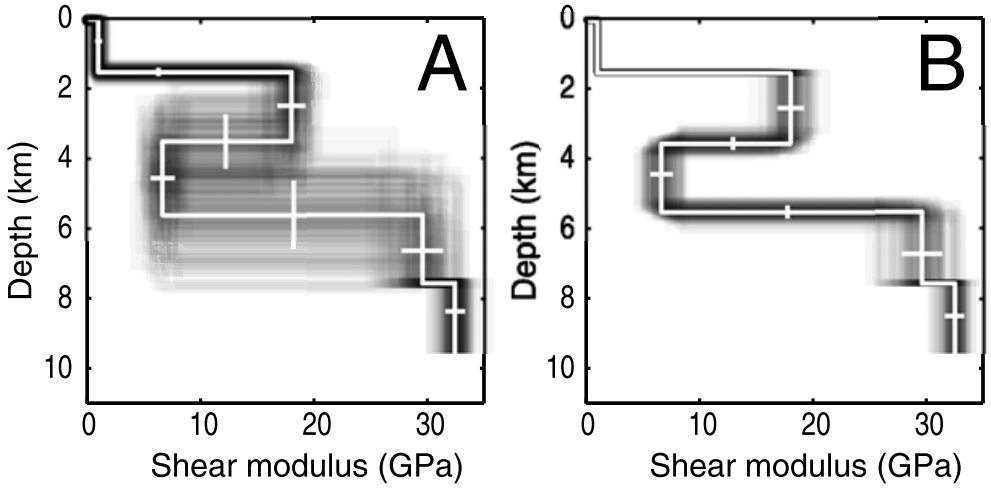

Figure 8. Results of 120 Bayesian inversions of seafloor compliance calculated using the reference model plus random data and *a priori* model noise. Density plot of all models (grey lines); model averages and standard deviations (white lines). (a) Starting models. (b) Inverted models.

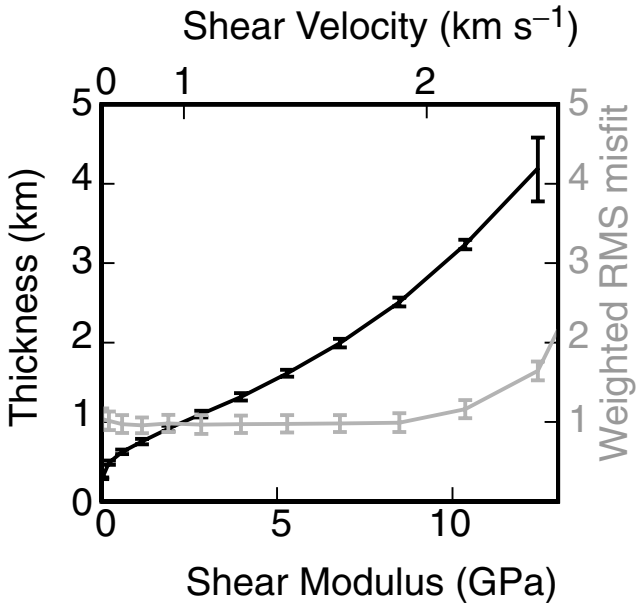

Figure 9. Sub-basalt sediment layer thickness–velocity combinations fitting seafloor compliances calculated from the reference model. Black symbols show the mean and standard deviation of layer thicknesses fitting the data for each shear modulus. Grey symbols show weighted RMS data misfits.

to 0.2 km and the shear modulus uncertainty in the second sediment layer decreases from 0.28 to 0.002 GPa. The basalt and basement shear moduli are poorly constrained because the moduli are relatively high.

The sub-basalt sediment shear modulus is also poorly constrained, but for a different reason: the effect of the shear modulus is hard to separate from the effect of the layer thickness on the seafloor compliance data. Shear moduli from 0.02 to 12.4 GPa will fit the reference model seafloor compliance data, with each shear modulus value requiring a different layer thickness (Fig. 9). A thin sub-basalt sediment layer with lower shear modulus generates a similar seafloor compliance as a thicker layer with higher shear modulus. Because the shear modulus of the layer is much more tightly constrained than its boundary depths in the *a priori* model, the inversion mostly changes the boundary depths. If these depths were previously constrained, we could constrain the shear modulus. If neither the depths nor the shear velocity is constrained, seafloor compliance measurements only constrain the modulus as a function of thickness.

Fig. 10 compares the seafloor compliance peaks generated by each of the best-fitting shear-modulus—layer-thickness pairs from Fig. 9. Most of the differences between the peaks are at the lowest frequencies where the seafloor compliance is not measured or weakly constrained. If the peak were centred at a higher frequency, that is, if the sub-basalt sediments were shallower or the water was deeper, the measured seafloor compliance would better separate the layer thickness from the shear modulus.

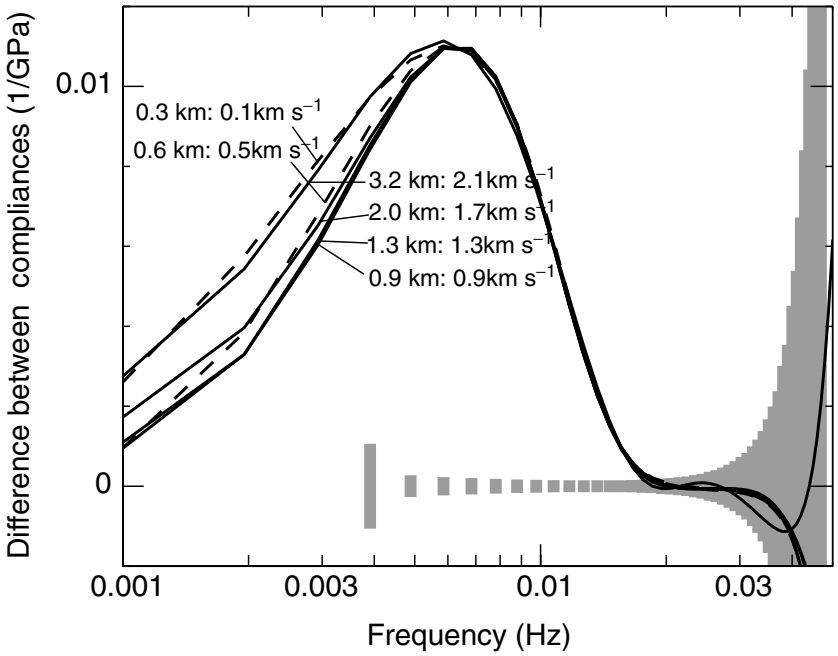

Figure 10. Seafloor compliance peaks created by the sub-basalt sediment thickness–velocity combinations shown in Fig. 9. Solid lines show seafloor compliance for sediment velocities $\geq$0.9 km s^{-1}, dashed lines are for sediment velocities $\leq$0.5 km s^{-1}. Grey vertical lines show seafloor compliance measurement uncertainties.

4.3 The effect of the different model parameters

To generalize our results for a wide range of possible sites, we calculated the effect of the water depth, wave strength and subsurface structure on the seafloor compliance sensitivity to sub-basalt sediments. To do so, we modified one parameter at a time from the reference model and then ran 100 Bayesian inversions for each new model. Table 3 shows the variability between inversion results (the inversion uncertainty) for each model.

We used another parameter to quantify seafloor compliance sensitivity: the thinnest sub-basalt sediment layer that a seafloor compliance measurement can detect. To determine this parameter, we calculated synthetic seafloor compliance data for different sub-basalt sediment layer thicknesses and then ran inversions in which no sub-basalt sediments are allowed. As before, we ran 100 inversions for each model, each time recalculating the noise in the starting model and seafloor compliance data. For each layer thickness, we then calculated the mean and variance of the weighted RMS data misfits. We consider that seafloor compliance measurements detect the sub-basalt sediments if the weighted RMS data misfit is more than one standard deviation above 1.0. For example, seafloor compliance detects sub-basalt sediments if they are 0.6 km or more thick when the rest of the model is the same as the reference model (Fig. 11).

Seafloor compliance sensitivity increases as the sub-basalt sediment shear modulus decreases. If we decrease the sub-basalt sediment shear modulus from 6.8 to 4.0 GPa (decreasing β from 1.6 to 1.3 km s^{-1}), the layer depth uncertainty decreases to 0.1 km and the minimum detectable layer thickness decreases to 0.4 km. If we increase the shear modulus to 10.4 GPa ($\beta = 2.1$ km s^{-1}), the depth uncertainty increases to 0.3–0.4 km s^{-1} and the minimum detectable layer thickness increases to 1.0 km.

The average shear modulus of the basalt layer has only a small effect on the seafloor compliance sensitivity, as long as the sub-basalt shear modulus is lower than the average basalt layer shear modulus. If we increase the basalt layer shear modulus from 18 to 48 GPa, the depth uncertainty to the top of the sub-basalt sediments decreases to 0.1 km s^{-1}, the size of the smallest detectable reservoir decreases to 0.4 km and the depth uncertainty to the bottom of the sub-basalt sediments does not change. If we decrease the basalt layer shear modulus to 11 GPa ($\beta = 2.1$ km s^{-1}), the depth uncertainty to the top of the layer increases to 0.4 km, the size of the smallest detectable reservoir increases to 1.5 km and the depth uncertainty to the bottom of the sub-basalt sediments does not change.

The thickness and shear velocity of the surface sediments have little effect on the seafloor compliance sensitivity. To determine this, we replaced the surface sediments with basalts of the same thickness and reran the inversions. The depth sensitivity to the top and bottom of the sub-basalt layer did not change and the minimum detectable thickness decreased slightly, to 0.5 km.

Increasing the source wave energy increases the seafloor compliance sensitivity. If the wave energy increases by a factor of 10 from the reference model (to 10^5Pa^2 Hz), the depth uncertainty to the sub-basalt sediment boundaries decreases to 0.1–0.2 km and the minimum detectable layer thickness decreases to 0.4 km. If the wave energy decreases to 10^3 Pa^2 Hz, the depth uncertainty increases to 0.3 km and the minimum detectable layer thickness increases to 1.0 km.

The longer the compliance sensor is deployed, the smaller the data uncertainty and the better the sensitivity. This improvement is most notable in the first few days of the experiment, because the data uncertainty decreases by the square root of the deployment length (eq. 8). If

Table 3. The effect of different parameters on the sensitivity of seafloor compliance to sub-basalt sediments. Constraints that are improved from the reference model are shown in bold text, weakened constraints are underlined.

	Depth uncertainty to top of sub-basalt sediments (km)	Depth uncertainty to bottom of sub-basalt sediments (km)	Minimum detectable thickness (km)
Reference model	*0.2*	*0.2*	*0.6*
Remove sediments above basalts (replace with basalt)	0.2	0.2	**0.5**
Decrease sub-basalt sediment μ to 4.0 GPa	**0.1**	**0.1**	**0.4**
Increase sub-basalt sediment μ to 10.4 GPa	*0.3*	*0.4*	*1.0*
Decrease basalt μ to 11 GPa	*0.4*	0.2	*1.5*
Increase basalt μ to 48 GPa	**0.1**	0.2	**0.4**
Decrease infragravity wave energy to 10^3 Pa^{2}Hz	*0.3*	*0.3*	*1.0*
Increase infragravity wave energy to 10^5 Pa^{2}Hz	0.2	**0.1**	**0.4**
Decrease water depth to 0.25 km	*0.5*	*0.8*	*1.2*
Increase water depth to 2 km	0.2	**0.1**	*0.7*
Decrease deployment length to 1 day (20 good windows)	0.2	*0.3*	*0.8*
Increase deployment length to 10 days (780 good windows)	0.2	**0.1**	**0.4**

we decrease the deployment cycle from two days to one day (20 data windows), the depth uncertainty to the layer bottom increases to 0.3 km and the minimum detectable layer thickness increases to 0.8 km. If we increase the deployment cycle to 10 days (780 data windows), the depth uncertainty to the layer bottom decreases to 0.1 km and the minimum detectable layer thickness decreases to 0.4 km.

The water depth affects the depth sensitivity of seafloor compliance measurements. The sub-basalt sediments in the reference model, which start 3.5 km beneath the seafloor, would be better constrained if the water were deeper. We ran inversions for water depths ranging from 0.05 to 5.0 km (Fig. 12). If the water is shallower than 0.1 km, seafloor compliance is insensitive to the sub-basalt sediments in the reference model. The depth uncertainty to the top of the layer is 1.0 km at 0.1-km water depth and decreases to a minimum of 0.2 km at 0.6-km water depth. The uncertainty levels off between 0.6- and 3-km water depth and increases again at greater depth. The uncertainty in depth to the bottom of the sub-basalt sediments decreases from 1.0 km at 0.1-km water depth to 0.2 km by 1.0-km water depth and decreases slightly at greater water depths, never passing below 0.1 km.

4.4 The relationship between the water depth and the sub-basalt reservoir depth

One of the most important factors determining if seafloor compliance can be used to study sub-basalt sediments at a site is the relationship between the sub-basalt sediment layer depth and the water depth. If the water is too shallow compared with the layer depth, the seafloor compliance will give no information about the sub-basalt sediments. If the water is too deep, the resolution may be compromised. One can easily calculate if seafloor compliance will be sensitive to a sub-basalt sediment layer at a given depth using the rule of thumb that seafloor compliance is sensitive to structures at approximately $1/5$ the water wavelength. Therefore, seafloor compliance can detect a sub-basalt sediment layer if the longest infragravity waves used in the measurement are at least five times longer than the depth to the top of the layer. For seafloor compliance to be sensitive to the entire layer, the longest infragravity wave should be at least five times longer than the depth to the bottom of the layer. The minimum water depth, $H_{\min}$, required to detect a sub-basalt reservoir whose top is D_t km beneath the seafloor is

$$H_{\min} \approx D_t^2/25, \tag{19}$$

assuming a minimum seafloor compliance frequency of 0.004 Hz and the shallow water ($k_w H \ll 1$) limit of eq. (4). Therefore, for the reference model ($D_t = 3.5$ km), the water depth should be at least 0.5 km to detect the sub-basalt sediments and 1.2 km to best constrain the depth to their top and bottom (this agrees with Fig. 12). The maximum water depth, $H_{\max}$, at which seafloor compliance is sensitive to structure at the top of the reservoir is

$$H_{\max} \approx 4.5 D_t, \tag{20}$$

because the shortest wavelength detected at the seafloor corresponds is $1.1H$. For the reference model, $H_{\max} = 15.8$ km.

5 CONCLUSIONS

The sensitivity of seafloor compliance measurements to sub-basalt sediments depends mostly on the sediment layer shear modulus and on the relationship between the sediment layer depth and the water depth. The deeper the water is, the longer the source waves will be and the

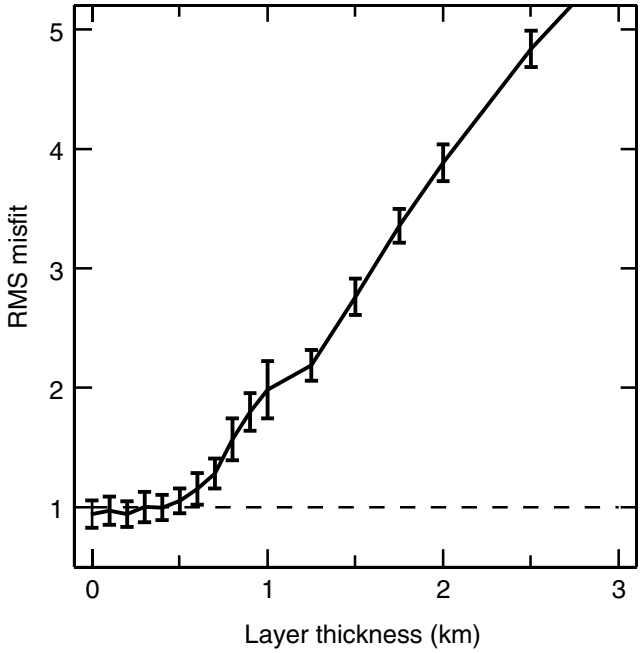

Figure 11. Weighted RMS data misfits, for inversions that do not allow a sub-basalt sediment layer, of data calculated for different sub-basalt sediment layer thicknesses. All of the other model parameters are the same as in the reference model. Error bars correspond to one standard deviation. Seafloor compliance detects the sub-basalt sediments if the misfits are more than one standard deviation greater than 1.0.

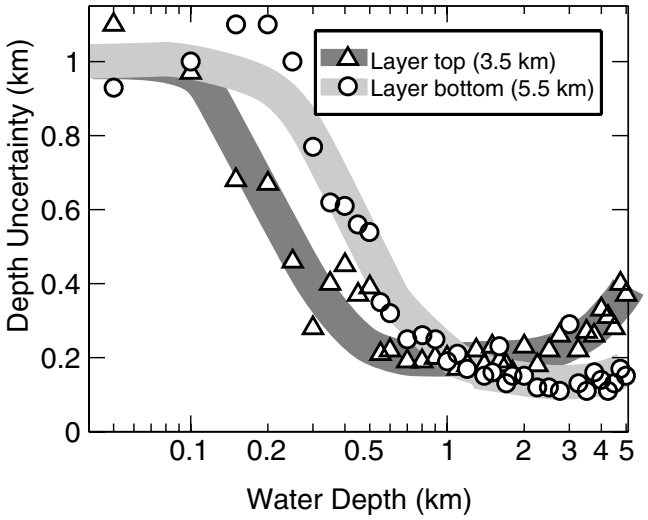

Figure 12. Depth uncertainty to the top and bottom of the reference model sub-basalt sediment layer as a function of water depth. Symbols show standard deviation of inversion results for each water depth, thick curves highlight trends. The *a priori* uncertainties are 1.0 km.

deeper the structure that seafloor compliance measurements will be sensitive to. The lower the shear modulus of the sub-basalt sediments, the better they will be constrained. Seafloor compliance measurements often constrain the relationship between the sub-sediment shear modulus and thickness rather than either parameter individually.

For a two-day seafloor compliance measurement with 10^4 Pa^2 Hz infragravity wave power spectral density over our reference model [sub-basalt sediments starting 3.5 kmbsf, with an average shear modulus of 6.8 GPa ($\beta \approx 1.7$ km s^{-1})] sub-basalt sediments at least 0.6-km thick will be detected at water depths greater than 1 km and sediments more than 1.2-km thick will be detected at water depths greater than 0.25 km. If the sub-basalt sediments are 2-km thick, seafloor compliance measurements in 1–3 km water depth will constrain the depth to their top and bottom to within 0.2 km. If the water is 0.25-km deep, seafloor compliance measurements will constrain these depths to within 0.5–0.8 km.

Other factors affecting the seafloor compliance sensitivity are:

(i) The infragravity wave energy: measured infragravity wave power spectral densities range from $IG = 10^{2.5}$–$10^{5.2}$ Pa^{2}Hz. The sensitivity to sub-basalt sediments increases with increasing infragravity wave energy.

(ii) The thickness of the sub-basalt sediment layer: the thicker the sub-basalt sediment layer, the larger will be the seafloor compliance peak it generates and the better the layer properties will be constrained.

(iii) The shear modulus contrast between the basalt layer and the sub-basalt sediments: the larger the contrast, the better the sub-basalt sediments will be constrained.

(iv) The deployment length: the data uncertainty is divided by the square root of the number of data windows, so longer deployments give better data. The measurement time is usually 12 to 18 hr shorter than the deployment length. We usually deploy the seafloor compliance sensors for at least 42 hr at each site to obtain approximately 100 1024-s data windows.

For the reference model at 1.3-km water depth and varying only one parameter at a time, the minimum detectable sub-basalt sediment thickness is: 0.4 km for $IG = 10^3$ and 1.0 km for $IG = 10^5$; 0.4 km for $\mu_{\text{basalt}} = 48$ GPa and 1.5 km for $\mu_{\text{basalt}} = 11$ GPa; and 0.4 km for a 10-day deployment and 0.8 km for a 1-day deployment. These changes in sensitivity will be different for different water depths or different subsurface structures and should be recalculated for each site.

The thickness and elastic parameters of any sediments above the basalt layer do not affect the sensitivity of seafloor compliance measurements to sub-basalt sediments and seafloor compliance measurements are insensitive to small-scale interlayering of basalt flows and sediments.

ACKNOWLEDGMENTS

The author thanks Satish Singh for suggesting the sub-basalt problem, Tom Hulme and Satish Singh for reading and discussing the manuscript, and Ruedi Widmer-Schniedrig and Torsten Dahm for insightful reviews. The authors is also grateful to the LITHOS consortium for financial support and travel to the 2002 Sub-Basalt Imaging conference at Cambridge, UK. Graeme Cairnes inspired the Bayesian data treatment and gave many useful references. This paper is IPGP contribution #1951.

REFERENCES

Aki, K. & Richards, P.G., 1980. *Quantitative Seismology: Theory and Methods,* W. H. Freeman and Company, San Francisco, p. 932.

Apel, J.R., 1987. *Principles of ocean physics,* Academic Press, London.

Beauduin, R., Lognonné, P., Montagner, J.P., Cacho, S., Karczewski, J.F. & Morand, M., 1996. The effects of the atmospheric pressure changes on seismic signals or How to improve the quality of a station, *Bull. seism. Soc. Am.,* **86**(6), 1760–1769.

Bendat, J.S. & Piersol, A.G., 1986. *Random Data: Analysis and Measurement Procedures,* John Wiley and Sons, New York, p. 566.

Bradley, C.R., Stephen, R.A., Dorman, L.M. & Orcutt, J.A., 1997. Very low frequency (0.2–10.0 Hz) seismoacoustic noise below the seafloor, *J. geophys. Res.,* **102**(6), 11 703–11 718.

Collins, J.A., Sutton, G.H. & Ewing, J.I., 1996. Shear-wave velocity structure of shallow-water sediments in the East China Sea, *J. acoust. Soc. Am.,* **100**(6), 3646–3654.

Collins, J.A., Vernon, F.L., Orcutt, J.A., Stephen, R.A., Peal, J.R., Hildebrand, J.A. & Spiess, P.N., 1998. Relative performance of the borehole, surficially-buried, and seafloor broadband seismographs on the ocean Seismic Network pilot experiment: frequency-domain results, *EOS, Trans. Am. geophys. Un.,* **79**(45), 661.

Constable, S.C., Parker, R.L. & Constable, C.G., 1987. Occam's inversion: a practical algorithm for generating smooth models from electromagnetic sounding data, *Geophysics,* **52,** 289–300.

Cox, C.S., Deaton, T. & Webb, S.C., 1984. A deep sea differential pressure gauge, *J. Atmos. oceanic Technol.,* **1,** 237–246.

Crawford, W.C., 1994. Determination of oceanic crustal shear velocity structure from seafloor compliance measurements, *PhD thesis,* University of California, San Diego, p. 96.

Crawford, W.C. & Webb, S.C., 2000. Removing tilt noise from low frequency (<0.1 Hz) seafloor vertical seismic data, *Bull. seism. Soc. Am.,* **90**(4), 952–963.

Crawford, W.C., Webb, S.C. & Hildebrand, J.A., 1991. Seafloor compliance observed by long-period pressure and displacement measurements, *J. geophys. Res.,* **96**(10), 16 151–16 160.

Crawford, W.C., Webb, S.C. & Hildebrand, J.A., 1998. Estimating shear velocities in the oceanic crust from compliance measurements by two-dimensional finite difference modeling, *J. geophys. Res.,* **103**(5), 9895–9916.

Crawford, W.C., Webb, S.C. & Hildebrand, J.A., 1999. Constraints on melt in the lower crust and Moho at the East Pacific Rise, 9°48′ N, using seafloor compliance measurements, *J. geophys. Res.,* **104**(2), 2923–2939.

Dorman, L.M., 1997. Propagation in marine sediments, in *Encyclopedia of Acoustics,* pp. 409–416, ed. Crocker, M.J., John Wiley and Sons, Inc., New York.

Fliedner, M.M. & White, R.S., 2001. Sub-basalt imaging in the Faeroe-Shetland Basin with large-offset data, *First Break,* **19,** 247–252.

Fruehn, J., White, R.S., Fliedner, M., Richardson, K.R., Cullen, E., Latkiewicz, C., Kirk, W. & Smallwood, J.R., 1999. Large-aperture seismic: Imaging Beneath High-Velocity Strata, *World Oil,* **Jan.,** 109–112.

Gatliff, R.W., Hitchen, K., Ritchie, J.D. & Smythe, D.K., 1984. Internal structure of the Erlend Tertiary volcanic complex, north of Shetland, revealed by seismic reflection, *J. Geol. Soc.,* **141,** 555–562.

Gomberg, J.S. & Masters, T.G., 1988. Waveform modeling using locked-mode synthetic and differential seismograms: application to determination of the structure of Mexico, *Geophys. J.,* **94,** 193–218.

Hamilton, E.L., 1976. Shear-wave velocity versus depth in marine sediments: a review, *Geophysics,* **41**(5), 985–996.

Hasselmann, K., 1963. A statistical analysis of the generation of microseisms, *Rev. Geophys.,* **1**(2), 177–210.

Hobbs, R., 2002. Sub-basalt imaging using low frequencies, *J. Conference Abstracts,* **7**(2), 152–153.

Hughes, S., Barton, P.J. & Harrison, D.J., 1997. Characterizing the Mid-Faeroe Ridge using seismic velocity measurements, *J. geophys. Res.,* **102**(4), 7837–7847.

Hughes, S., Barton, P.J. & Harrison, D., 1998. Exploration in the Shetland-Faeroe Basin using densely spaced arrays of ocean-bottom seismometers, *Geophysics,* **63**(2), 490–501.

Jackson, D.D. & Matsu'ura, M., 1985. A Bayesian approach to nonlinear inversion, *J. geophys. Res.,* **90**(1), 581–591.

Jegen, M., Hautot, S., Cairns, G. & Tarits, P., 2002. Using electromagnetics to image sub-basalt sediments, *J. Conference Abstracts,* **7**(2), 154–155.

Latychev, K. & Edwards, R.N., 2003. On the compliance method and the assessment of three dimensional sea floor gas hydrate deposits, *Geophys. J. Int.,* **155**(3), 923–952.

Longuet-Higgins, M.S., 1950. A theory for the generation of microseisms, *Phil. Trans. R. Soc. Lond., A.,* **243,** 1–35.

MacGregor, L.M. & Sinha, M.C., 2002. Sub-basalt imaging using marine controlled source electromagnetic sounding, *J. Conference Abstracts,* **7**(2), 172–173.

Mack, H., 1997. Seismic response of Tertiary basalt flows in Northeast Atlantic—a modelling study. In: *EAGE 59th Conference and Technical Exhibition,* Paper B017.

Mudge, D. & Rashid, B., 1987. The geology of the Faeroe Basin area, in, *Petroleum Geology of northwest Europe,* pp. 751–763, eds Brooks, J. & Glennie, K., Graham and Trotman, London.

Murphy, C.A., 2002. Resolving basalt and sub-basalt geology with high precision high resolution gravity gradient data, *J. Conference Abstracts,* **7**(2), 178–179.

Ogilvie, J.S., Crompton, R. & Hardy, N.M., 2001. Characterization of volcanic units using detailed velocity analysis in the Atlantic Margin, West of Shetlands, United Kingdom, *Leading Edge,* **Jan.**, 34–50.

Okihiro, M., Guza, R.T. & Seymour, R.J., 1992. Bound infragravity waves, *J. geophys. Res.,* **97**(C7), 11 453–11 469.

Parker, R.L., 1994. *Geophysical Inverse Theory,* Princeton University Press, Princeton, NJ, p. 386.

Ridd, M.F., 1981. Petroleum geology west of the Shetlands, in *Petroleum Geology of the Continental Shelf of NW Europe,* pp. 414–425, eds Illing, L.V. & Hobson, G.D., Institute of Petroleum, London.

Stephen, R.A., Collins, J.A., Hildebrand, J.A., Orcutt, J.A., Peal, K.R., Spiess, F.N. & Vernon, F.L., 1999. Seafloor seismic stations perform well in study, *EOS, Trans. Am. geophys. Un.,* **80**(49), 592.

Stoll, R.D., 1977. Acoustic waves in ocean sediments, *Geophysics,* **42**(4), 715–725.

Tinivella, U. & Accaino, F., 2000. Compressional velocity structure and Poisson's ratio in marine sediments with gas hydrate and free gas by inversion of reflected and refracted seismic data (South Shetland Islands, Antarctica), *Mar. Geol.,* **164,** 13–27.

Webb, S.C., 1992. The equilibrium oceanic microseism spectrum, *J. acoust. Soc. Am.,* **92**(4), 2141–2158.

Webb, S.C., 1998. Broadband seismology and noise under the ocean, *Rev. Geophys.,* **36**(1), 105–142.

Webb, S.C. & Crawford, W.C., 1999. Long period seafloor seismology and deformation under ocean waves, *Bull. seism. Soc. Am.,* **89**(6), 1535–1542.

Webb, S.C., Zhang, X. & Crawford, W.C., 1991. Infragravity waves in the deep ocean, *J. geophys. Res.,* **96**(C2), 2723–2736.

White, R.S., Fruehn, J., Richardson, K.R., Culen, E., Kirk, W., Smallwood, J.R. & Latkiewicz, C., 1999. Faeroes large aperture research experiment (FLARE): imaging through basalt, in *Petroleum Geology of Northwest Europe: Proceedings of the 5th Conference,* pp. 1243–1252, eds Fleet, A.J. & Boldy, S.A.R., Geological Society, London.

Yamamoto, T. & Torii, T., 1986. Seabed shear modulus profile inversion using surface gravity (water) wave-induced bottom motion, *Geophys. J. R. astr. Soc.,* **85,** 413–431.

Yamamoto, T., Trevorrow, M.V., Badiey, M. & Turgut, A., 1989. Determination of the seabed porosity and shear modulus profiles using a gravity wave inversion, *Geophys. J. Int.,* **98**(1), 173–182.

Ziolokowski, A., Hanssen, P., Gatliff, R., Li, X.-Y., Jakubowicz, H. & Hampson, G., 2002. Use of low frequencies for sub-basalt imaging, *J. Conference Abstracts,* **7**(2), 202–203.

APPENDIX A: SEAFLOOR COMPLIANCE OF A UNIFORM HALF-SPACE

We start with the stress–strain relationship for a linearly elastic and isotropic medium:

$$\tau_{ij} = \lambda u_{l,l}\delta_{ij} + \mu(u_{i,j} + u_{j,i}) \tag{A1}$$

and the corresponding equation of motion

$$\rho\ddot{\mathbf{u}} = (\lambda + 2\mu)\nabla(\nabla \cdot \mathbf{u}) - \mu\nabla \times (\nabla \times \mathbf{u}) \tag{A2}$$

where u is displacement, τ_{ij} is the i component of stress acting on a surface whose normal points in the x_j-direction, μ is the shear modulus and λ is the dilatation modulus. We can represent $\mathbf{u}$ using Helmholtz potentials

$$\mathbf{u} = \nabla\varphi + \nabla \times \mathbf{\Psi} \tag{A3}$$

and substitution into eq. (A2) gives

$$\begin{aligned} \frac{\partial^2\varphi}{\partial t^2} &= \frac{\lambda + 2\mu}{\rho}\nabla^2\varphi = \alpha^2\nabla^2\varphi \\ \frac{\partial^2\Psi}{\partial t^2} &= \frac{\mu}{\rho}\nabla^2\mathbf{\Psi} = \beta^2\nabla^2\mathbf{\Psi}, \end{aligned} \tag{A4}$$

where α is the compressional velocity and β is the shear velocity. For plane wave forcing in the x-direction (SV waves) with wavenumber k, we set $\varphi = \varphi\,(z)e^{i(\omega t + kx)}$ and $\Psi = \Psi\,(z)e^{i(\omega t + kx)}$ to give

$$\begin{aligned} \frac{d^2\varphi}{dz^2} &= (k^2 - \omega^2/\alpha^2)\varphi \\ \frac{d^2\mathbf{\Psi}}{dz^2} &= (k^2 - \omega^2/\beta^2)\mathbf{\Psi}. \end{aligned} \tag{A5}$$

The solution to these equations is:

$$\begin{aligned} \varphi(z) &= ae^{rz} + be^{-rz}: \quad r = \sqrt{k^2 - \omega^2/\alpha^2} = k\sqrt{1 - c_w^2/\alpha^2} \\ \Psi(z) &= \mathbf{c}e^{sz} + \mathbf{d}e^{-sz}: \quad s = \sqrt{k^2 - \omega^2/\beta^2} = k\sqrt{1 - c_w^2/\beta^2}. \end{aligned} \tag{A6}$$

If the phase speed of the water waves $c_w \equiv \omega/k$ is less than α and β, then r and s are real and the motion exponentially decays or grows with depth. If c_w is greater than α and β, then r and s are imaginary and the waves are propagating. Because the forcing is planar, $\mathbf{c}$ and $\mathbf{d}$ can be replaced by scalars.

Seafloor compliance is the seafloor displacement divided by the seafloor pressure

$$\xi|_{z=0} = \frac{\mathbf{u}}{\tau_{zz}} = \frac{u_x\hat{x} + u_z\hat{z}}{\lambda u_{x,x} + (\lambda + 2\mu)u_{z,z}}, \tag{A7}$$

with the boundary conditions that $\tau_{zx} = 0$ at the seafloor (free slip) and that there is no motion at infinite depth (b and $\mathbf{d} = 0$ in eq. A6). To find the values of a and $\boldsymbol{c}$ and hence evaluate the expression of eq. (A7), we use eqs (A3) and (A1) to write the displacement and stresses in terms of the solutions in eq. (A6):

$$\mathbf{u} = i(ake^{rz} + \boldsymbol{c}se^{sz})e^{(\cdot)}\hat{x} + (are^{rz} + \boldsymbol{c}ke^{sz})e^{(\cdot)}\hat{z}, \tag{A8}$$

$$\begin{aligned}\tau_{zz} &= \{[(\lambda + 2\mu)r^2 - \lambda k^2]ae^{rz} + 2\mu sk\boldsymbol{c}e^{sz}\}e^{(\cdot)} \\ \tau_{xz} &= [2rkae^{rz} + (s^2 + k^2)\boldsymbol{c}e^{sz}]e^{(\cdot)}.\end{aligned} \tag{A9}$$

The seafloor compliance is then

$$\xi|_{z=0} = \frac{i(ka + s\boldsymbol{c})\hat{x} + (k\boldsymbol{c} + ra)\hat{z}}{\{[(\lambda + 2\mu)r^2 - \lambda k^2]a + 2\mu ks\boldsymbol{c}\}}. \tag{A10}$$

The free-slip boundary condition at the seafloor gives

$$c = \frac{-2kr}{(s^2 + k^2)}a, \tag{A11}$$

which results in

$$\xi|_{z=0} = \frac{ik(s^2 + k^2 - 2rs)\hat{x} + r(s^2 - k^2)\hat{z}}{(s^2 + k^2)[(\lambda + 2\mu)r^2 - \lambda k^2] - 4\mu k^2 sr}. \tag{A12}$$

To simplify this expression, we assume that $\boldsymbol{c}_w \ll \alpha$, $\beta$and use the Taylor expansions

$$r = k\left(1 - \frac{\rho \boldsymbol{c}_w^2}{2(\lambda + 2\mu)} + \text{h.o.t.}\right) \tag{A13}$$

$$s = k\left(1 - \frac{\rho \boldsymbol{c}_w^2}{2\mu} + \text{h.o.t.}\right), \tag{A14}$$

to obtain

$$\xi|_{z=0} = \frac{-i}{2k(\lambda + \mu)}\hat{x} + \frac{(\lambda + 2\mu)}{2k\mu(\lambda + \mu)}\hat{z}. \tag{A15}$$

Because the wavenumber k, depends on the water depth and the frequency, we use the normalized seafloor compliance, $\eta \equiv k\xi|_{z=0}$, which depends only on the material parameters:

$$\eta = \frac{-i}{2(\lambda + \mu)}\hat{x} + \frac{(\lambda + 2\mu)}{2\mu(\lambda + \mu)}\hat{z}. \tag{A16}$$